Progress In Electromagnetics Research Letters, Vol. 104, 27–35, 2022

Bandpass Filters Based on Hybrid Structure of Substrate Integrated Waveguide (SIW) and Hilbert Defected Ground Structure (HDGS)

Mohammed El Amine Chaib[1], Mehadji Abri[1], Hadjira Badaoui[1], and Nabil Cherif[2, *]

Abstract—In this article, two compact Substrate Integrated Waveguide (SIW) bandpass filters based on Defected Ground Structure (DGS) technology are proposed. Hilbert Cell of second order is the resonator shape proposed for the DGS of both filters, where the first filter DGS consists of five pairs, and the second one uses only three pairs. The pair used in the first filter consists of two cells located side to side whereas they are placed face to face in the second filter. In order to enhance the performance of the second filter and based on the evanescent-mode technique, three other pairs of first order Hilbert cells are engraved on the top layer. Both bandpass filters are designed to operate in C band with a measured bandwidth of 1.8 GHz for the first filter and 0.86 GHz for the second one. The proposed structures have the same physical dimensions, which is 38.1 mm × 16 mm with different measured insertion losses of −2.5 dB and −2.7 dB. Both structures exhibit an upper stopband rejection with attenuation around −20 dB and −29 dB, respectively. The filters operate in a transmission bandwidth of [5.5 GHz—7.3 GHz] and [5.27 GHz–6.13 GHz] with a fractional bandwidth (FBW) of 28.1% and 15.09% for the first filter and the second filter, respectively. A good agreement is reported between the measured and simulated results.

1. INTRODUCTION

The rapid development of telecommunication systems in recent years has created a competition among the different companies specialized in this field, and this concurrence is mainly based on the latest academic researches. Microwave devices design is one of the main areas of interest of researchers, whose researches are based on reducing components size, minimizing losses, and low cost. In contrast to the limited performance of traditional stepped impedance microstrip filters, SIW technology offers improved filter specifications that meet the requirements of modern communication systems [1]. SIW technology has come to meet these needs, which offers as advantages of the reduction of size, low-cost and high Q-factor [2]. Based on these advantages, SIW technology has become a candidate in numerous components design as filter, coupler, diplexer, and antennas [3].

Recently, the appearance of Defected Ground Structure (DGS) Technology has attracted considerable attention. By etching a lot of forms on the Ground of structure, the frequency response of devices can be changed. Hilbert form is one of the fractal forms used in DGS [4]. Based on space filling Peono curve, the German mathematician David Hilbert proposed the Hilbert fractal curve in 1891 [5]. It became one of the most space-filling curves used in many research areas [6]. The fractal Hilbert curves, for the first time, were explored in antenna geometry by [7]. After that, their applications were extended for the other components. The advantage of using a Hilbert curve as a resonator is that we can get diverse responses simply by varying line-to-spacing ratio and the orientation of the curve [8, 9]. To improve the performance of components, Many papers have treated the combination between SIW

Received 25 March 2022, Accepted 2 May 2022, Scheduled 11 May 2022

* Corresponding author: Nabil Cherif (nabil.cherif@univ-mascara.dz).

[1] STIC Laboratory, Department of Telecommunications, Abou Bekr Belkaid University, Tlemcen 13000, Algeria. [2] LSTE, Mascara University, Algeria.

and DGS [10, 11]. To ensure a good adaptation between SIW and planar circuits, several types of transitions have been proposed for this purpose. In our case, we have exploited as transitions: stepped transition [12] and taper transition, which has been recently proposed in [13].

In this paper, two bandpass filters are proposed. In both designs, the same SIW cavity is used, but the main difference was focused on the number, type, orientation, and location of Hilbert cells etched in DGS and also the transitions used to link the SIW with the microstrip circuit. The design and simulation of the both filters have been done based on CST (Computer Simulation Technology) software. In order to give a credibility to the proposed designs, both filters have been fabricated and measured.

The next parts of this article are organized as follows. Section 2 presents SIW theory as well as an overview of the Hilbert fractal forms employed in DGS for both filters. Section 3 is dedicated to the detailed description of the filters design followed by a comparison between simulated and measured results, and the discussions will be addressed in Section 4.

2. SIW THEORY AND HILBERT CURVE OVERVIEW

2.1. The Substrate Integrated Waveguide

SIW structure consists of dielectric material with top and bottom metallic surfaces embedded in it. The inclusion of two linear arrays of conductor vias connecting the top and bottom of the SIW distinguishes it from conventional planar waveguides as shown in Figure 1.

In terms of propagation, SIW structures behave like a dielectric-filled waveguide (DFW) [14].

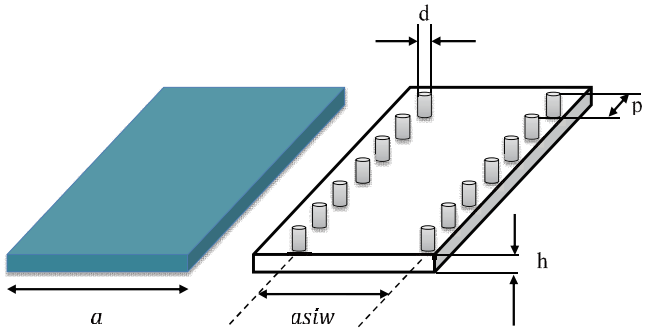

Figure 1. Dielectric filled waveguide (DFW) with SIW configurations.

Each waveguide propagation mode has a cutoff frequency, provided by [15]:

$$f_{cmn} = \frac{c}{2\sqrt{\varepsilon_r}}\sqrt{\left(\frac{m}{a}\right)^2 + \left(\frac{n}{b}\right)^2} \tag{1}$$

Taking the dominant mode TE_{10}, we have:

$$f_{c10} = \frac{c}{2a\sqrt{\varepsilon_r}} \tag{2}$$

where c is the velocity of light in free space, and a is the width of DFW. The SIW design is mainly based on the cylinder diameter (d) and the distance between the vias (p) [16], and both parameters are conditioned by the following equations [16]:

$$d = \lambda_g/5 \tag{3}$$

$$d < p \leq 2d \tag{4}$$

where λ_g is the guided wavelength, defined by:

$$\lambda_g = \frac{2\pi}{\sqrt{\frac{(2\pi f)^2 \varepsilon_r}{c^2} - (\pi/a)^2}} \tag{5}$$

SIW design is conditioned by the following relations [17, 18]:

$$L = L_{siw} - \frac{d^2}{0.95p} \tag{6}$$

$$a = a_{siw} - \frac{d^2}{0.95p} \tag{7}$$

Substituting Equation (7) in Equation (2), finally, we get:

$$f_{c10} = \frac{c}{2\sqrt{\varepsilon_r}} \left(a_{siw} - \frac{d^2}{0.95p} \right)^{-1} \tag{8}$$

As we have already mentioned in the introduction, both proposed filters used the same SIW Cavity based on an FR-4 substrate with relative permittivity $\varepsilon_r = 4.3$. The dimensions selected to design the SIW cavity are as follows: $h = 1.6\,\text{mm}$, $d = 1\,\text{mm}$, $p = 1.5\,\text{mm}$, $W_{siw} = 13.38\,\text{mm}$, $L_{siw} = 21.5\,\text{mm}$.

2.2. Hilbert Unit Cell Curve

Like every fractal curve, Hilbert curves change from one stage to the next stage based on the iterations of original geometry (Figure 2). Hence, the geometry of a desired stage can be obtained just by assembling four copies of the preceding order iteration [19].

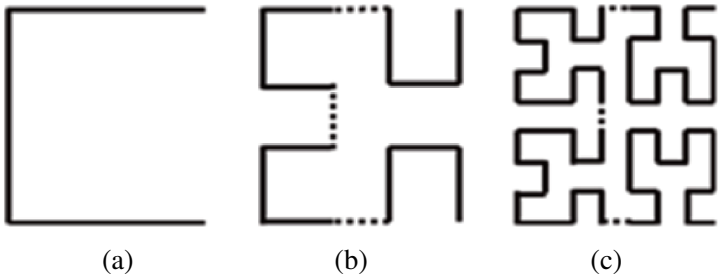

Figure 2. Hilbert Forms generation: (a) first order, (b) second order and (c) third order.

In this paper, we use the first and second orders Hilbert cells. The adequate cells dimensions depicted in Figure 3 were obtained after optimization on CST.

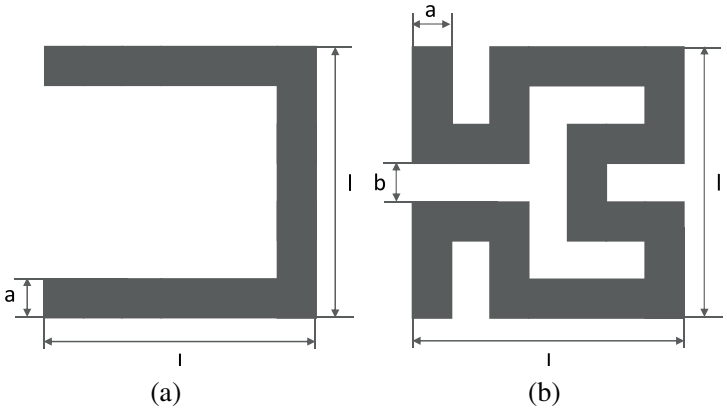

Figure 3. The unit cells used in filter design, (a) first order cell and (b) second order cell, $a = b = 0.5\,\text{mm}$ and $l = 3.5\,\text{mm}$.

3. FILTERS DESIGN

3.1. Operating Principle of Proposed Filters

Both proposed filters have been designed to meet the following specifications: C band operating frequency, passband return loss $< -20\,\text{dB}$, passband insertion loss $> -3\,\text{dB}$, and stopband rejection $> 20\,\text{dB}$.

Figure 4 illustrates the operating principle of our proposed structures. As known from the literature [20], SIW structure provides a high pass response filter. On the other hand, a structure can work as a bandstop filter by etching Hilbert cells on the bottom metal side (GND) [21]. As a final response, a bandpass response can be achieved just by combining the previous two structures.

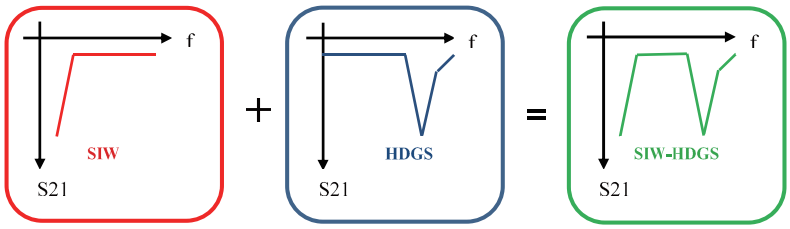

Figure 4. Operating principle of proposed pass-band filters.

3.2. First Proposed Filter

Figure 5 shows the schematic of the first filter. It consists of a SIW cavity with five pairs of second order Hilbert fractal unit cells etched on the bottom metal layer with identical period $eh = 1.5\,\text{mm}$ and spaced vertically by $ev = 2.4\,\text{mm}$. In order to get a good adaptation, a stepped impedance transitions line [12] with optimized dimensions is used to link the SIW with the 50 ohms microstrip line.

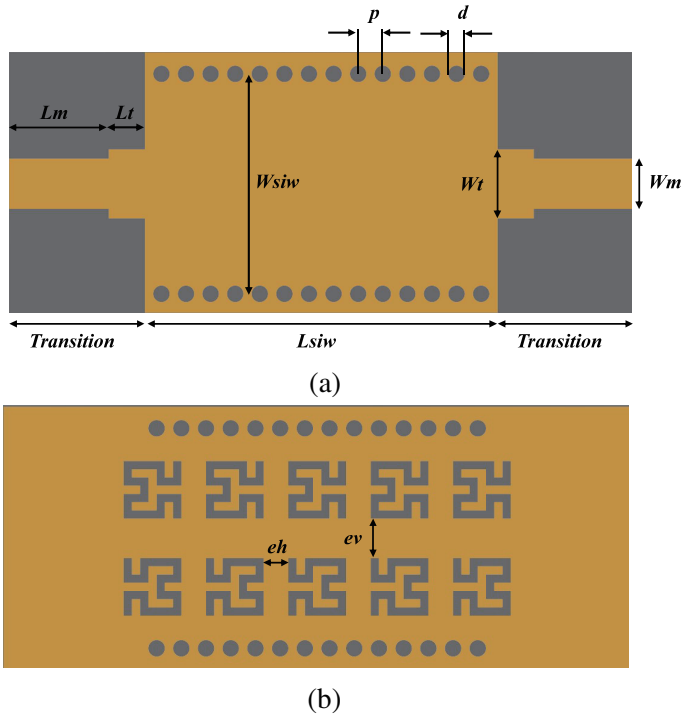

Figure 5. Schematic of the first proposed filter, (a) top view, (b) bottom view. $W_t = 4.2\,\text{mm}$, $L_t = 2.21\,\text{mm}$, $W_m = 3.06\,\text{mm}$, and $L_m = 6.1\,\text{mm}$.

3.3. Second Proposed Filter

In this filter, the same topology of the first filter (Five pairs of 2nd order Hilbert cells) was used but the cells location were selected to be placed face to face. However, the unsatisfactory result led us to use only three pairs, but eventually the obtained result of this proposal did not also get much better. Finally, the result was ameliorated based on the evanescent mode propagation technique [22], which was applied by engraving three other pairs of first order Hilbert cells on the top layer.

All cells' placements have been chosen to be face to face and separated horizontally and vertically by $eh = 4.5$ and $ev = 0.6\,\text{mm}$, respectively (Figure 6).

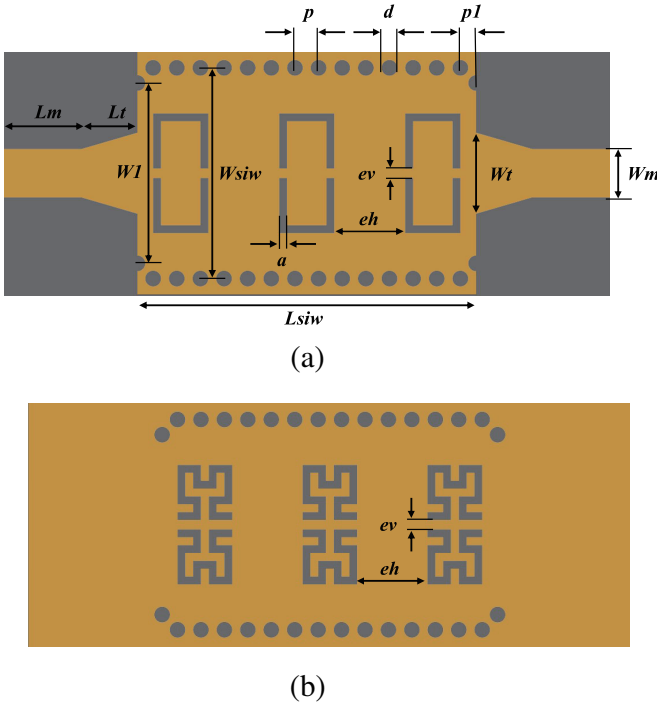

Figure 6. Schematic of the second proposed filter, (a) top view, (b) bottom view.

To get an adequate adaptation, a taper of dimension ($L_t \times W_t$) is used to link the SIW circuits with the 50 microstrip line of dimensions $L_m \times W_m$. The size of this taper has been calculated (Table 1) based on following Equations (9) and (10) defined in [13]:

$$W_t = W_m + 0.1547 a_{siw} \tag{9}$$

$$L_t = 0.2368 \lambda_{g-siw} \tag{10}$$

$$\lambda_{g-siw} = \frac{\lambda_{g0}}{\sqrt{\varepsilon_{reff}}} \tag{11}$$

where λ_{g0} is the guided wavelength in free space and ε_{reff} the effective permittivity. In each side of the taper to SIW transition and in order to compensate the reactance effects of this junction [13], we added

Table 1. Dimensions of transition used in second filter.

Parameters	Value (mm)	Parameters	Value (mm)
$p1$	0.98	Wt	5.13
$W1$	11.45	Lm	5
Lt	3.55	Wm	3.06

two symmetric vias which are positioned based on the following equations:

$$p_1 = 0.6567p \tag{12}$$

$$W_1 = 0.8556a_{siw} \tag{13}$$

4. RESULTS DISCUSSION

To demonstrate the proposed bandpass filters, both structures were designed and optimized based on CST software. As a validation of the obtained layouts described above, each prototypes has been fabricated and tested. Figure 11 illustrates the measurement operation where an Agilent 8719ES vector network analyzer is used. Photographs of the fabricated filters are presented in Figure 7 and Figure 9, where their total sizes are $1.32\lambda_g \times 0.56\lambda_g$ and $1.18\lambda_g \times 0.49\lambda_g$, respectively.

The comparisons between the simulated (dashed line) and measured (solid line) results are depicted in Figure 8 and Figure 10. It is clear that there is a good agreement where both filters exhibit passband. The small shift in obtained results is due to the inaccuracy of the PCB dielectric constant and the additional loss of the SMA connector. Both filters present a bandpass behavior of a bandwidth of 1.8 GHz and 0.86 GHz, with a center frequency of 6.4 GHz and 5.7 GHz, respectively for the first filter and second filter. Both structures have measured in-band insertion losses less than 3 dB, and they have maximum measured in-band return losses around −32 dB and around −33.7 dB for the first and second

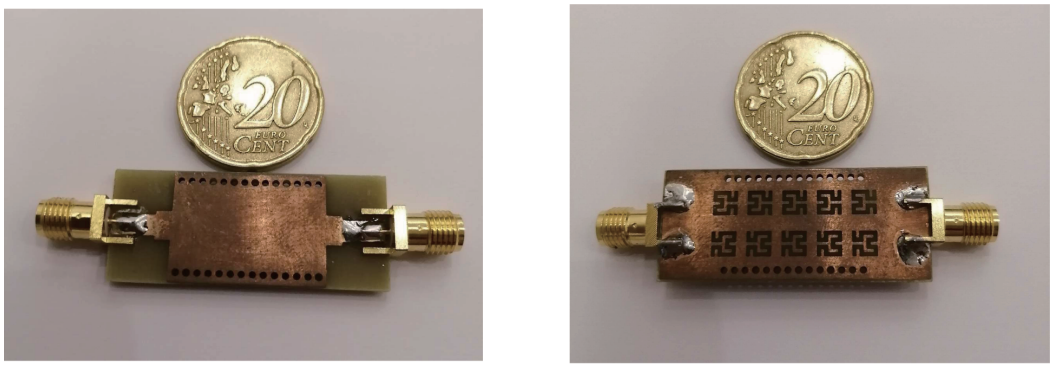

Figure 7. Photograph of first prototype, (a) top view and (b) bottom view.

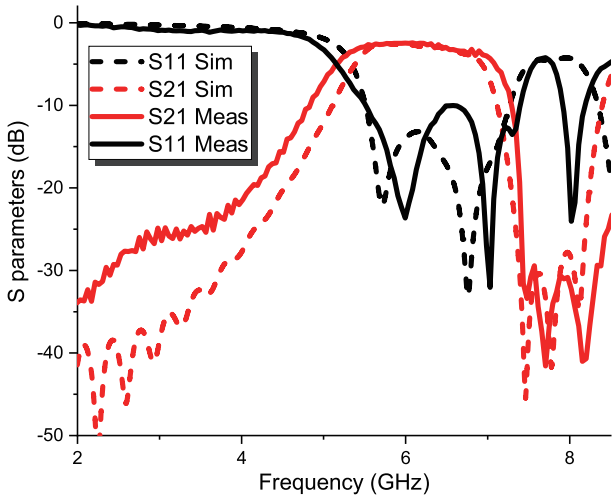

Figure 8. Simulated and measured results of first filter.

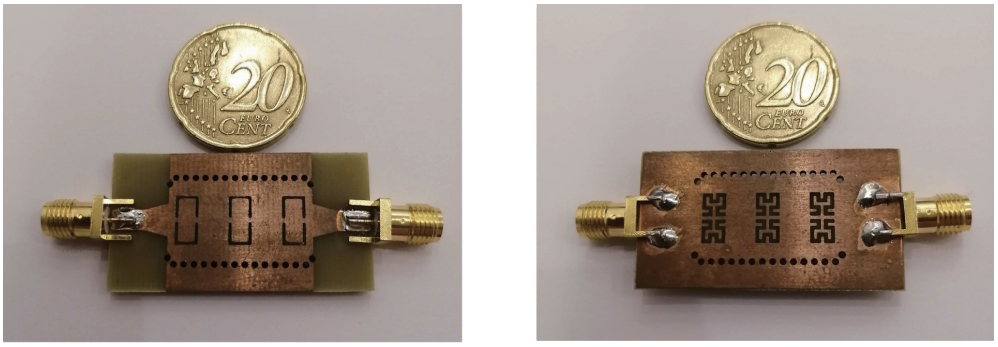

(a) (b)

Figure 9. Photograph of second prototype, (a) top view and (b) bottom view.

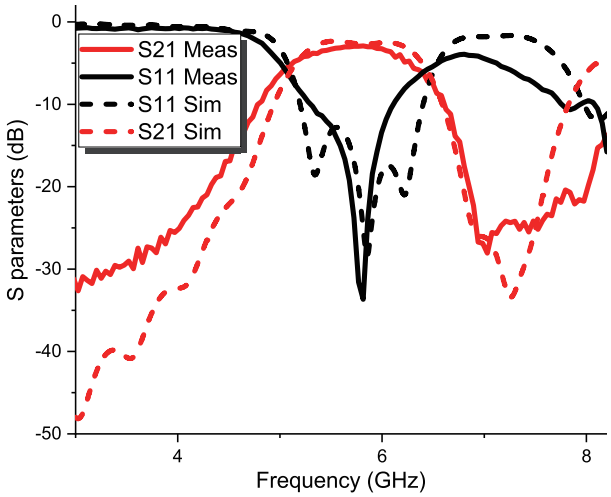

Figure 10. Simulated and measured results of second filter.

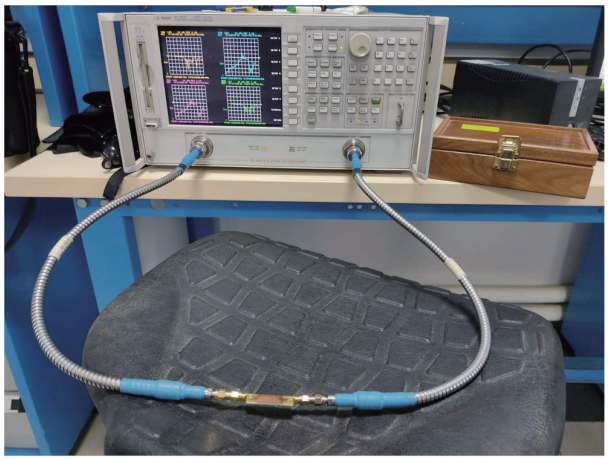

Figure 11. Photograph of measurement operation.

cases, respectively. The upper stopband is associated with three TZs located at 7.48 GHz, 7.7 GHz, and 8.15 GHz, respectively for the first filter and only one TZ located at 6.98 GHz for the second filter. The attenuation is greater than 29 dB and 20 dB over a frequency range of [7.4 GHz–8.33 GHz] and [6.84 GHz–

8 GHz] respectively for the first prototype and the second prototype. Based on the measured return losses mentioned above, the calculated fractional bandwidths (FBWs) are respectively 28.1% and 15.09 %, which means that the first filter works in wide-band range.

Table 2 represents the proposed filters performance compared with some previous SIW works.

Table 2. Results comparison with other references.

Ref	Center frequency (GHz)	FBW (%)	RL (dB)	IL (dB)	Size λ_g^2
[11]	6.7	22.7	34	2.6	0.62
[23]	3.4	25	11.4	1.7	0.45
[24]	3.7	16	18	1.1	1.34
[25]	9.97	14.75	16.7	1.65	1.1
[26]	8.98	47.4	18	11.5	1.18
[27]	6.88	40	16.5	2	1.69
This work (1)	6.4	28.1	32	2.5	0.74
This work (2)	5.7	15.09	33.7	2.7	0.58

5. CONCLUSION

In this paper, we present two novel BPF filters based on hybrid structure of Substrate Integrated Waveguide (SIW) and Hilbert Defected Ground Structure (HDGS). To connect SIW to microstrip circuit, a stepped transition and taper transition were used. The two filters have the same size 38.1 mm × 16 mm and operate over bandwidths of 1.8 GHz and 860 MHz, respectively, which makes them appealing to the new technology industry that focuses on miniaturization, integration and performance.

REFERENCES

1. Zhang, W., W.-M. Yang, Y.-Y. Fang, C.-K. Hu, X.-Y. Zhu, and G. Ma, "Design of the Hilbert fractal defected ground structure low-pass filter," *IEEE International Conference on Communiction Problem-solving (ICCPS 2014)*, 99–102, Beijing, China, Dec. 2014.
2. Rayas-Sanchez, J. E. and V. Gutierrez-Ayala, "A general EM-based design procedure for single-layer substrate integrated waveguide interconnects with microstrip transitions," *IEEE MTT-S International Microwave Symposium Digest (MWSYM 2008)*, 983–986, Atlanta, GA, USA, Jun. 2008.
3. Sahu, A., V. K. Devabhaktuni, R. K. Mishra, and P. H. Aaen, "Recent advances in theory and applications of substrate-integrated waveguides: A review," *Int. J RF Microw. Comput. Aided Eng.*, Vol. 26, No. 2, 129–145, Oct. 2015.
4. Yan, D., X. Zeng, and K. Zhang, "HDGS bandsyop filter design by FGA," *IEEE Youth Conference on Information, Computing and Telecommunications (YCICT 2010)*, 5–8, Beijing, China, Nov. 2010.
5. Sagan, H., *Space-filling Curves*, Springer-Verlag, New York, 1994.
6. Zhu, J., A. Hoorfar, and N. Engheta, " Bandwidth, cross-polarization, and feed-point characteristics of matched Hilbert antennas," *IEEE Antennas and Wireless Propagation Letters*, Vol. 2, No. 2, 2–5, 2003.
7. Vinoy, K. J., K. A. Jose, V. K. Varadan, and V. V. Varadan, "Hilbert curve fractal antenna: A small resonant antenna for VHF/UHF applications," *Microwave Opt. Technol. Lett.* Vol. 29, No. 4, 215–219, May 2001.
8. Zemlyakov, K. N. and V. Crnojević-Bengin, "Electronically tunable fractal microstrip resonatorsand filters," *The 10th International Conference on Telecommunication in Modern Satellite Cable and Broadcasting Services (TELSIKS 2011)*, 525–528, Nis, Serbia, Oct. 5–8, 2011.

9. Ghosh, B., D.-H. Yang, J.-C. Cheng, and J. S. Fu, "Bandpass characteristics of substrate integrated waveguide loaded with Hilbert curve fractal slot," *IEEE International Workshop on Electromagnetics, Applications and Student Innovation (IWEM 2011)*, 89–93, Taipei, Taiwan, 2011.
10. Fellah, B., N. Cherif, M. Abri, and H. Badaoui, "CSRR-DGS bandpass filter based on half mode substrate integrated waveguide for X-band applications," *Advanced Electromagnetics*, Vol. 10, No. 3, 39–42, Nov. 2021.
11. Noura, A., M. Benaissa, M. Abri, H. Badaoui, T. Vuong, and J. Tao, "Miniaturized half-mode SIW band-pass filter design integrating dumbbell DGS cells," *Microw. Opt. Technol. Lett.*, Vol. 61, 1473–1477, 2019.
12. Nouri, K., K. Haddadi, O. Benzaïm, T. Lasri, and M. Feham, "Substrate integrated waveguide (SIW) inductive window band-pass filter based on post-wall irises," *Eur. Phys. J. Appl. Phys.* Vol. 53, No. 3, 2011.
13. Kordiboroujeni, Z. and J. Bornemann, "New wideband transition from microstrip line to substrate integrated waveguide," *IEEE Transactions on Microwave Theory and Techniques*, Vol. 62, No. 12, 2983–2989, Nov. 20, 2014.
14. Bozzi, M., A. Georgiadis, and K. Wu, "Review of substrate-integrated waveguide circuits and antennas," *IET Microw. Antennas Propag.*, Vol. 5, No. 8, 909–920, Jun. 2011.
15. Pozar, D. M., *Microwave Engineering*, Wiley, Amherst, MA, 1998.
16. Deslandes, D. and K. Wu, "Design consideration and performance analysis of substrate integrated waveguide components," *The 32nd European Microwave Conference (EUMA 2002)*, 881–884, Milan, Italy, Oct. 4–6, 2002.
17. Cassivi, Y., L. Perregrini, P. Arcioni, M. Bressan, K. Wu, and G. Conciauro, "Dispersion characteristics of substrate integrated rectangular waveguide," *IEEE Microwave and Wireless Components Letters*, Vol. 12, No. 9, 333–335, Sep. 2002.
18. Xu, F. and K. Wu, "Guided-wave and leakage characteristics of substrate integrated waveguide," *IEEE Transactions on Microwave Theory and Technique*, Vol. 53, No. 1, 66–73, Jan. 2005.
19. Chen, J., Z.-B. Weng, Y.-C. Jiao, and F.-S. Zhang, "Lowpass filter design of hilbert curve ring defected ground structure," *Progress In Electromagnetics Research*, Vol. 70, 269–280, 2007.
20. Mahant, K. and H. Mewada, "Substrate integrated waveguide based dual-band bandpass filter using split ring resonator and defected ground structure for SFCW Radar applications," *Int. J. RF Microw. Comput. Aided Eng.*, Vol. 28, No. 9, Oct. 2018.
21. Ahn, D., J.-S. Park, C.-S. Kim, J. Kim, Y. Qian, and T. Itoh, "A design of the low-pass filter using the novel microstrip defected ground structure," *IEEE Transactions on Microwave Theory and Techniques*, Vol. 49, No. 1, 86–93, Jan. 2001.
22. Dong, Y. D., T. Yang, and T. Itoh, "Substrate integrated waveguide loaded by complementary split ring resonators and its application to miniaturized waveguide filters," *IEEE Trans. Microw. Theory Tech.*, Vol. 57, No. 9. 2211–2223, Sep. 2009.
23. De Dios Ruiz, J., F. L. Martínez-Viviente, A. Alvarez-Melcon, and J. Hinojosa, "Substrate integrated waveguide (SIW) with Koch fractal electromagnetic bandgap structures (KFEBG) for bandpass filter design," *IEEE Microw. Wireless Compon. Lett.*, Vol. 25, No. 3, 160–162, Mar. 2015.
24. Wong, S.-W., R.-S. Chen, J.-Y. Lin, L. Zhu, and Q.-X. Chu, "Substrate integrated waveguide quasi-elliptic filter using slot-coupled and microstrip-line cross-coupled structures," *IEEE Trans. Compon. Packag. Manuf. Technol.*, Vol. 6, No. 12, 1881–1888, Dec. 2016.
25. Moitra, S. and P. S. Bhowmik, "Analyse of combined DSRR and EBG structure over SIW and HMSIW for obtaining band pass response," *Wireless Personal Communications*, Vol. 111, No. 2, 1207–1218, 2019.
26. Liu C. and X. An, "A SlW-DGS wideband band-pass filter with a shape roll-off at upper stop band," *Microw. Opt. Technol. Lett.*, Vol. 59, 789–792, 2017.
27. Jin, J.-D. and D.-H. Yu, "Substrate integrated waveguide band-pass filter with coupled complementary split ring resonators," *General Assembly and Scientific Symposium, IEEE*, 1–4, 2014.